Molecular Transition Metal Oxides: Ab Initio and Density Functional Electronic Structure Study of Tungsten Oxide Clusters

Athanassios C. Tsipis and Constantinos A. Tsipis*

Laboratory of Applied Quantum Chemistry, Faculty of Chemistry, Aristotle University of Thessaloniki, 540 06 Thessaloniki, Greece

Received: August 10, 1999; In Final Form: November 11, 1999

First principles quantum chemical calculations at the HF, MP2, and B3LYP levels of theory, using the LANL2DZ basis set, have been used to explore the potential energy hypersurfaces (PESs) of tungsten(VI) oxide species of molecular dimensions, formulated as WO_3, WO_4^{2-}, WO_4H_2, WO_4Na_2, $W_2O_5^{2+}$, and W_2O_6. The energetics of all topomers corresponding to global or local minima and saddle points in the potential energy hypersurfaces were computed at the more sophisticated QCISD(T) level. The proton affinity of the WO_4^{2-} dianion was found to be equal to 1584, 1593, and 1586 kJ mol^{-1} at the MP2, B3LYP, and QCISD(T) levels of theory. The formation process of W_2O_6 by dimerization of WO_3 species was predicted to be exothermic, the energy of formation being equal to 127.8, 100.3, 107.6, and 109.1 kcal·mol^{-1} at the HF, MP2, B3LYP, and QCISD(T) levels, respectively. Finally, the computed spectroscopic properties (harmonic vibrational frequencies and corresponding normal modes, electronic transitions and NMR chemical shifts) of the molecular tungsten oxides are thoroughly discussed in relation with available experimental data.

1. Introduction

Transition metal oxides have been extensively studied in their bulk states, but despite substantial interest from a catalytic perspective, our knowledge of simple metal oxide molecules is far from complete.[1] Over the past several years[2−6] considerable attention has been devoted to studies of the chemistry of such metal oxides generated by laser ablation of metal + oxygen systems or solid metal oxides, or produced in a plasma environment. The interest stems from the expectation that these studies may provide insight into many important processes such as catalysis, vapor deposition, and the formation and growth of metal oxide particles and powders which find many applications. Moreover, the intrinsic behavior of these species with regard to the evolution of condensed phase properties distinct from those in the gas phase is also of interest. Experiments on transition metal oxide clusters were focused on the determination of the composition, building blocks, abundance patterns, and fragmentation routes of the clusters. In addition, infrared, Raman, and photoelectron spectroscopies have been extensively used to investigate the structural parameters, vibrational frequencies, electron affinities, bonding, and electronic structure properties of small clusters.

Interest in the specific case of tungsten oxide is stimulated by its catalytic activity toward different reactions[7−9] from its structural, electronic, ferroelectric, electrochromic, and semiconducting properties[10,11] and from the tungsten bronzes (insertion compounds).[12−14] Furthermore, new forms of tungsten oxides of molecular dimensions, arranged into open framework, layer, and tunnel structures have recently been synthesized within the void structure of the zeolite Y host.[15−18] The experimental data regarding the irreversibly anchored exclusively in the large α-cage transition metal oxides prompt us to investigate through first principles computational techniques the structural, energetic, electronic, and spectroscopic properties of the various types of molecular tungsten oxides. In particular, we report on the details of modeling molecular tungsten oxide ions and clusters, by means of high level ab initio quantum chemical and density functional methods, pursuing a four-fold objective: (i) The determination of the ground states and their structural parameters. (ii) The understanding of the bonding properties of the molecular tungsten oxides. (iii) The interpretation of the computed harmonic vibrational frequencies and corresponding normal modes, as well as the UV−Vis electronic transitions and magnetic shielding tensors in relation with available experimental and other theoretical data. (iv) The exploration of the relative stability of the molecular tungsten oxides.

2. Computational Details

The geometry of the tungsten oxides studied was fully optimized at three different levels of theory, namely the single determinant Hartree−Fock (HF), the correlated MP2, and the Becke 3-parameter hybrid functional combined with the Lee−Yang−Parr correlation functional (B3LYP) level of theory, using the LANL2DZ basis set that includes Dunning/Huzinaga full DZ on first row and Los Alamos ECPs plus DZ for W atom. In all computations no constraints were imposed on the geometry. Full geometry optimization was performed for each complex structure using standard analytical gradient techniques, and the attainment of the energy minimum was verified by calculating the vibrational frequencies that result in the absence of negative eigenvalues. The vibrational modes and the corresponding frequencies are based on a harmonic force field. Moreover, single-point calculations at the more sophisticated QCISD(T) level of theory were performed on the optimized geometries at the MP2 and B3LYP levels. All calculations were performed with the *Gaussian 94* series of programs.[19] Magnetic shieldings have been computed with the GIAO (gauge-including atomic orbitals) DFT method as implemented in the *Gaussian*

* To whom correspondence should be addressed. Telephone: (+031) 997851. Fax: (+031) 997851. E-mail: tsipis@chem.auth.gr

10.1021/jp992814b CCC: $19.00
Published on Web 01/07/2000

TABLE 1: Geometrical, Energetic, and Electronic Properties of the Trigonal Pyramidal Ground State $WO_3(C_{3v})$ and the Trigonal Planar Transition State $WO_3(D_{3h})$ Species Calculated at Various Levels of Theory

method	r(W−O) (Å)	∠OWO (°)	∠OWOO (°)	energy (Hartree)	ZPE (kcal/mol)	q(W)	q(O)
$WO_3(C_{3v})$							
HF	1.716	110.7	123.2	−291.6399	5.77	1.810	−0.603
MP2	1.807	103.8	108.1	−292.3750	5.11	1.769	−0.590
B3LYP	1.746	106.9	114.1	−293.5414	5.42	1.268	−0.423
QCISD(T)				−292.2981		1.769	−0.590
$WO_3(D_{3h})$							
HF	1.726	120.0	180.0	−291.6253	5.26	1.845	−0.615
MP2	1.810	120.0	180.0	−292.3279	4.51	1.854	−0.618
B3LYP	1.756	120.0	180.0	−293.5095	4.86	1.337	−0.446
QCISD(T)				−292.2639		1.854	−0.618

94 series of programs[19] employing the B3LYP level of theory and corresponding to absolute magnetic shielding tensors. Electronic transitions have been computed by means of the CI−singles approach.

3. Results and Discussion

3.1. Structural, Energetic, Electronic, and Vibrational Properties of Molecular Tungsten Oxide Clusters. The computed structural, energetic, and electronic properties of molecular tungsten oxide clusters will be discussed separately for each tungsten oxide in the following subsections.

3.1.1. WO_3. The computed structural, energetic, and electronic properties of the WO_3 species at various levels of first principles quantum chemical calculations are summarized in Table 1. The global minimum in the potential energy hypersurface of the WO_3 molecule corresponds to the trigonal pyramidal geometry exhibiting C_{3v} symmetry, as the optimized geometry has positive definite Hessian. The trigonal planar structure belonging to the D_{3h} point group posseses one imaginary frequency and therefore is an inversion transition state to the C_{3v} molecule, with the computed inversion barrier being equal to 9.16, 29.6, 20.1, and 21.5 kcal/mol at the HF, MP2, B3LYP, and QCISD(T) levels of theory, respectively. The equilibrium length of the W−O bond of both the ground and transition state of the WO_3 molecule at the HF level is less than the B3LYP one, while the MP2 level gives even longer bond length. However, the computed equilibrium bond distances of both the ground and transition state of the WO_3 molecule are in good agreement to other theoretical and experimental values of related solid-state species (cubic and tetragonal phases of bulk tungsten trioxide) containing W−O bonds found in the range of 1.79−1.83 Å (in the a direction), 1.76−2.17 Å (in the b direction), and 1.83−2.12 Å (in the c direction).[20−24] A recent ab initio HF study[11] of the cubic and tetragonal phases of bulk tungsten trioxide predicted equilibrium W−O bond lengths of 1.629 and 1.636 Å for the tetragonal WO_3 and 1.882 and 1.660 Å for the less stable cubic WO_3 at the HF and HF+corr level of theory, respectively. The computed O−W−O bond angles are 110.7, 103.8, and 106.9 at the HF, MP2, and B3LYP levels of theory, respectively, in comparison to the NLSDA value[25] of 115 for the CrO_3 species. The smaller O−W−O bond angle as compared to O−Cr−O bond angle could be the result of the decrease of the O−O repulsions, for the W−O bonds are longer than the Cr−O bond (NLSDA value[25] of 1.62 Å). The WO_3 moiety could be considered as the fragment resulting from the regular octahedral structural unit of the cubic phase of bulk WO_3 upon removing three facial oxygen atoms. Therefore, it is expected the WO_3 moiety to adopt a trigonal pyramidal (C_{3v}) rather than a trigonal planar (D_{3h}) geometry. In effect our ab initio calculations strongly support the trigonal pyramidal as the more stable structure for the WO_3 group. The observed stability of the C_{3v} conformer could be attributed to the increased covalent character of the W−O bonds with respect to the D_{3h} conformer. This is reflected on both the computed net atomic charges and bond populations computed by Mulliken population analysis. At all levels of theory both tungsten and oxygen atoms acquire lower net atomic charges in C_{3v} in relation to the D_{3h} conformer. The W−O bond overlap is 0.355 and 0.352 in C_{3v} and D_{3h} conformers, respectively. Moreover, it is the symmetry breaking that results in the increase of the tungsten−oxygen interaction involving orbitals of both σ and π symmetry along the W−O bonds. The C_{3v} conformer is a polar molecule, the computed dipole moment being equal to 6.34, 5.95, 7.92, and 7.92 D at the HF, MP2, B3LYP, and QCISD(T) levels of theory, respectively.

The predicted harmonic vibrational frequencies of the ground state WO_3 moeity are those expected for a trigonal pyramidal geometry of C_{3v} symmetry (totally 6 normal modes). The three high-frequency normal modes in the region of 925.5−992.5 cm^{-1} (reported values are those computed at the B3LYP level) could be assigned to ν(W−O) stretching vibrations of A_1 and E symmetry, while the three low-frequency ones in the region of 284.5−332.8 cm^{-1} could be assigned to δ(O−W−O) bending vibrations of A_1 and E symmetry as well. In general the B3LYP approach yielded higher harmonic vibrational frequencies than the MP2 one, in accordance with recent theoretical results concerning the vibrational frequencies of various small titanium/oxygen compounds.[21,22] The computed harmonic vibrational frequencies of the transition state are those expected for a trigonal planar geometry of D_{3h} symmetry (totally six normal modes). The three high-frequency normal modes in the region of 934.2−961.2 cm^{-1} could be assigned to ν(W−O) stretching vibrations of A_2' and E' symmetry, while the two low-frequency ones at 283.3 cm^{-1} could be assigned to δ(O−W−O) bending vibrations of E' symmetry. The A_2'' bending vibration exhibiting the negative eigenvalue occurs at −253.5 cm^{-1}. The δ(O−W−O) frequencies of the transition state are lower than the corresponding frequencies of the ground state, being possibly the result of the weakening of the W−O bonds in the transition state which become longer and more ionic.

3.1.2. WO_4^{2-}, WO_4H_2, and WO_4Na_2. The computed structural, energetic, and electronic properties of WO_4^{2-} dianions at various levels of first principles quantum chemical calculations are summarized in Table 2. The global minimum in the potential energy hypersurface of WO_4^{2-} species corresponds to the tetrahedral geometry of T_d symmetry, as vibrational frequency analysis indicated zero Hessian index at all theoretical levels considered in this study. The complementary square planar geometry belonging to the D_{4h} point group posseses one imaginary frequency and therefore is a transition state to the inversion process of the T_d molecule, with a high inversion barrier amounting to 159.3, 144.4, 147.0, and 148.2 kcal/mol

TABLE 2: Geometrical, Energetic, and Electronic Properties of the Tetrahedral Ground State $WO_4^{2-}(T_d)$ and the Square Planar Transition State $WO_4^{2-}(D_{4h})$ Species Calculated at Various Levels of Theory

method	r(W−O) (Å)	∠OWO (°)	∠OWOO (°)	energy (Hartree)	ZPE (kcal/mol)	q(W)	q(O)
WO_4^{2-} (T_d)							
HF	1.786	109.5	120.0	−366.5931	7.53	1.724	−0.931
MP2	1.860	109.5	120.0	−367.4211	6.41	1.750	−0.937
B3LYP	1.816	109.4	120.0	−368.8852	7.28	0.956	−0.739
QCISD(T)				−367.3744		1.750	−0.937
WO_4^{2-} (D_{4h})							
HF	1.834	90.0	180.0	−366.3392	6.46	1.525	−0.881
MP2	1.930	90.0	180.0	−367.1901	5.05	1.534	−0.884
B3LYP	1.864	90.0	180.0	−368.6510	6.82	0.698	−0.674
QCISD(T)				−367.3744		1.750	−0.937

TABLE 3: Geometrical, Energetic, and Electronic Properties of the Ground State $WO_4H_2(C_2)$ Species Calculated at Various Levels of Theory

property	MP2	B3LYP	QCISD(T)
r(W−O) (Å)	1.792	1.737	
r(W−OH) (Å)	1.898	1.860	
r(O−H) (Å)	0.968	0.965	
∠OWO (°)	103.2	105.7	
energy (Hartree)	−368.6287	−370.0986	−368.5827
ZPE (kcal/mol)	19.55	19.84	
q(W)	2.264	1.561	2.264
q(O)	−0.629	−0.447	−0.629
q(OH)	−1.006	−0.762	−1.006
q(H)	0.440	0.429	0.503

at the HF, MP2, B3LYP, and QCISD(T) levels of theory, respectively. For both the ground and transition state WO_4^{2-} species, the results illustrate the usual bond lengthening effect of electron correlation. The W−O bonds in the transition state are about 0.05−0.07 Å longer than the corresponding bonds of the ground state. This was also the case for the WO_3 molecule. In addition, the W−O bonds of WO_4^{2-} species are about 0.05−0.07 Å longer than the corresponding bonds of the WO_3 molecule. The W−O bonds in $WO_4^{2-}(D_{4h})$ species are more ionic than the corresponding bonds of the ground state $WO_4^{2-}(T_d)$ molecule. This is reflected on both the computed net atomic charges and bond populations computed by Mulliken population analysis. At all levels of theory both tungsten and oxygen atoms acquire higher net atomic charges in T_d in relation to the D_{4h} conformer. The W−O bond overlap is 0.361 and 0.312 in T_d and D_{4h} conformers, respectively.

The IR active, triply degenerate, high-frequency normal modes of the $WO_4^{2-}(T_d)$ dianion at 814.5 cm^{-1} could be assigned to ν(W−O) stretching vibrations of T_2 symmetry, while the triply degenerate low-frequency modes at 289.0 cm^{-1} could be assigned to δ(O−W−O) bending vibrations of T_2 symmetry, as well. The computed harmonic vibrational frequencies of the transition state are those expected for a square planar geometry of D_{4h} symmetry (totally nine normal modes). The vibrational frequencies of the $WO_4^{2-}(D_{4h})$ species are higher than the corresponding frequencies of the ground state $WO_4^{2-}(T_d)$ dianion, in line with the strengthening of the W−O bonds in the square planar transition state.

Upon protonation the dianion is converted to a neutral dihydroxy species, which adopts a C_2 configuration. The computed structural, energetic, and electronic properties of the ground state $WO_4H_2(C_2)$ molecule at various levels of first principles quantum chemical calculations are summarized in Table 3. The computed proton affinity of the $WO_4^{2-}(T_d)$ dianion is equal to 1584, 1593, and 1586 kJ mol^{-1} at the MP2, B3LYP, and QCISD(T) levels of theory, respectively. The W−O bond of the protonated oxygen atoms exhibits a longer bond length by 0.038 and 0.044 Å at the MP2 and B3LYP levels of theory, respectively, as compared to the respective bonds of the unprotonated species (Table 2). In contrast, the W−O bond of the unprotonated oxygen atom exhibits a shorter bond length by 0.068 and 0.079 Å at the same levels of theory, with respect to the corresponding bonds of the unprotonated species.

The protonation of the $WO_4^{2-}(T_d)$ dianion results in a significant increase of the positive net atomic charge on the tungsten central atom by 0.51, 0.61, and 0.51 unit charge at the MP2, B3LYP, and QCISD(T) levels, respectively. This charge density redistribution is followed by a concomitant decrease of the negative net atomic charge on the unprotonated oxygen atom by about 0.28, 0.29, and 0.11 unit charges at the MP2, B3LYP, and QCISD(T) levels of theory, respectively. In contrast, the negative net atomic charge on the protonated oxygen atoms increases by about 0.17, 0.02, and 0.07 unit charge at the same levels of theory.

The most important IR active vibrations of the ground state $WO_4H_2(C_2)$ molecule are those assigned to antisymmetric and symmetric stretching vibrations of the O−H bonds in the region of 3920−3925 cm^{-1}. The dipole moment, of the protonated species is calculated to be equal to 4.78, 3.74, and 4.78 D at the MP2, B3LYP, and QCISD(T) levels, respectively.

Considering that the $WO_4^{2-}(T_d)$ dianion is bound to Na^+ ions which are held within the zeolite framework, we have also investigated the WO_4Na_2 molecule aiming to understand the effects of clambing the oxygen atoms on the structural, electronic, and spectroscopic properties of the $WO_4^{2-}(T_d)$ moiety. The global minimum in the potential energy hypersurface of the WO_4Na_2 molecule corresponds to the structure belonging to the C_1 point group. The optimized $WO_4Na_2(C_1)$ structure computed at the B3LYP and MP2 levels of theory is shown in Figure 1. It is evident that clambing the oxygen atoms on the Na^+ ions lowers the symmetry of the $WO_4^{2-}(T_d)$ dianion to C_1. Interestingly the WO_4^{2-} dianion bounds to the two Na^+ ions in an η^2-type of bonding with the Na^+ ions sharing a common oxygen atom. The W−ONa bond involving the common oxygen atom exhibits a longer bond length by 0.05 Å as compared to the two other W−ONa bonds, while the terminal W−O bond is shorter by 0.05 Å with respect to the same bonds (Figure 1). This is also reflected in the bond populations computed by Mulliken population analysis. At the B3LYP and MP2 levels of theory the W−O bond overlap of the terminal oxygen atom is 0.368 and 0.348, those of the bridging W−O−Na oxygen atoms 0.290 and 0.280, and those of the triply bridged oxygen atom 0.238 and 0.221, respectively. The B3LYP and MP2 Na−O bond overlap is only 0.065 and 0.050, indicating a predominantly ionic character for the interaction of the oxygen atoms with Na^+ ions.

The clambing of the $WO_4^{2-}(T_d)$ dianion to Na^+ ions results in a significant charge density redistribution. The possitive net atomic charge on the tungsten central atom increases (1.949,

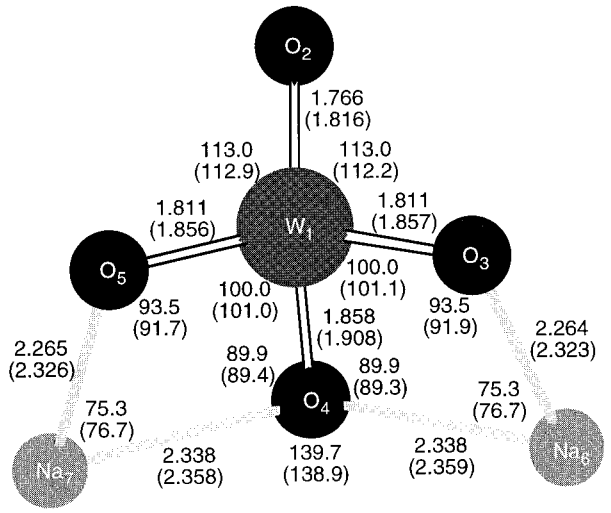

Figure 1. Optimized structure of the ground state $WO_4Na_2(C_1)$ molecule computed at the B3LYP and MP2 (figures in parentheses) levels of theory (bond lengths in Å, bond angles in degrees).

1.271, and 1.991 unit charges at the MP2, B3LYP, and QCISD-(T) levels, respectively) followed by a concomitant decrease of the negative net atomic charge on both the clambed and terminal oxygen atoms. The B3LYP and MP2 negative net atomic charges on the terminal oxygen atom are −0.556 and −0.750, those on the bridging W−O−Na oxygen atoms −0.732 and −0.928, and those of the triply bridged oxygen atom −0.864 and −1.075, respectively. Obviously, the triply bridged oxygen atom acquires the higher net atomic charge and therefore is the electrophilic center of the molecule. The computed dipole moment of $WO_4Na_2(C_1)$ is equal to 13.36, 12.84, and 12.99 D at the MP2, B3LYP, and QCISD(T) levels of theory, respectively.

The most important IR active vibrations of the ground state $WO_4Na_2(C_1)$ molecule are those assigned to W−O stretching involving the terminal oxygen atom at 933 cm^{-1}, W−O−Na bending deformations at 862 and 835 cm^{-1}, W−O stretching involving the triply bridged oxygen atom at 749 cm^{-1}, and skeletal deformations at 394 cm^{-1} and 356 cm^{-1}.

3.1.3. $W_2O_5^{2+}$. Two stationary points corresponding to C_1 and C_s topomers were located on the potential energy hypersurface of the $W_2O_5^{2+}$ dication. The C_1 topomer is the global minimum, as the optimized geometry has positive definite Hessian, whereas the C_s topomer possesses one imaginary frequency and is a rotational transition state to the C_1 topomer. Table 4 contains selected geometrical, energetic, and electronic parameters of the ground state topomer of C_1 symmetry. The computed structural, energetic, and electronic properties of the C_s transition state at the HF level are shown in Figure 2. The transition state exhibits noticeable structural and electronic differences with respect to the ground state and therefore the relatively high activation barrier (14 kcal/mol at the HF level) can be easily understood. The ground state C_1 topomer is a polar molecule, the computed dipole moment being equal to 6.48, 7.22, and 6.08 D at the HF, MP2, and B3LYP levels of theory, respectively. The bridging oxygen atom acquires the higher negative net atomic charge and therefore is the nucleophilic center of the molecule. In contrast, the nucleophilic center is localized on the W central atoms acquiring relatively high positive net atomic charges. The terminal t-W−O bonds in $W_2O_5^{2+}(C_1)$ dication are stronger than the bridging μ-W−O bonds. This is reflected in the bond populations computed by Mulliken population analysis. The bond overlap of the t-W−O bond is 0.359 in comparison to the bond overlap of μ-W−O which is only 0.129. The bond overlap

TABLE 4: Geometrical, Energetic and Electronic Properties of the Ground State $W_2O_5^{2+}(C_1)$ Species Calculated at Various Levels of Theory

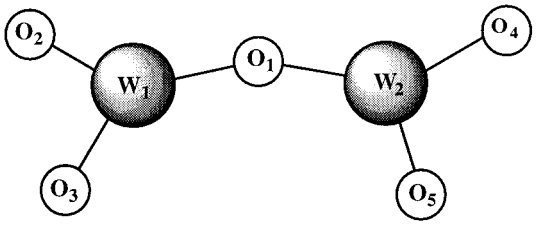

property	HF	MP2	B3LYP
$r(W_1-O_1)$ (Å)	1.884	1.916	1.896
$r(W_1-O_2)$ (Å)	1.663	1.765	1.702
$\angle O_1W_1O_2$ (°)	105.5	99.1	103.1
$\angle O_1W_1O_3$ (°)	106.3	98.1	103.2
$\angle O_2W_1O_3$ (°)	104.0	101.6	102.9
$\angle W_1O_1W_2$ (°)	167.4	156.8	161.9
$\angle O_1W_1O_2O_3$ (°)	111.0	101.1	107.1
$\angle O_2W_1O_1W_2$ (°)	104.7	96.0	93.2
$\angle O_3W_1O_1W_2$ (°)	5.4	7.3	13.7
energy (Hartree)	−507.7345	−509.0660	−511.0950
ZPE (kcal/mol)	9.98	11.29	10.53
q(W)	2.258	1.690	1.748
$q(O_1)$	−1.159	−0.792	−0.804
$q(O_2)$	−0.335	−0.156	−0.171
$q(O_3)$	−0.343	−0.138	−0.175

between the tungsten atoms is −0.013, showing a slight antibonding character and indicating that no metal−metal interactions are present in the dication.

The IR active normal modes of the $W_2O_5^{2+}(C_1)$ dication at 1053.2 cm^{-1} and 999.5 cm^{-1} are assigned to O−W−O rocking vibrations, while the absorption bands at 1001.4 cm^{-1} and 899.5 cm^{-1} are assigned to the skeleton wagging.

Finally, exploring further the potential energy hypersurface of the $W_2O_5^{2+}$ dication it was found that the structures belonging to D_{2d} and D_{2h} correspond to second- and third-order saddle points with their geometric, energetic, and electronic parameters shown in Figure 2. These structures are more than 30 kcal/mol higher in energy than the ground state at the HF level. The energy difference becomes even higher (almost doubled) at the B3LYP and MP2 levels of theory.

3.1.4. W_2O_6. The global minimun in the potential energy hypersurface of the W_2O_6 moiety corresponds to a D_{2h} structure. This species could be considered as the WO_3 dimer. From another point of view the D_{2h} structure could be seen as two tungstenate, WO_4^{2-} tetrahedrons linked together via an edge sharing with the tungsten atoms being separated by 2.98 Å. Table 5 contains selected geometrical parameters of the ground state W_2O_6 of D_{2h} symmetry, along with the total electronic energy and charge distribution computed at various levels of theory. The formation of a second O-bridge results in the lengthening of both the interior and terminal Ti−O bonds by about 0.05 and 0.03 Å, respectively. Moreover, there is a redistribution of the charge density resulting in a significant increase of the negative net atomic charge on the terminal O atoms amounting to 0.50−0.80 charge units at the various levels of computation and a concomitant decrease of the net atomic charges on both tungsten and bridging O atoms amounting to about 0.30 and 0.50 charge units, respectively. The dipole moment of W_2O_6 is predicted to be zero at all computational levels. The terminal t-W−O bonds in the $W_2O_6(D_{2h})$ molecule are stronger than the bridging μ-W−O bonds. This is reflected on the bond populations computed by Mulliken population analysis. The bond overlap of the t-W−O bond is 0.380 in comparison to the bond overlap of μ-W−O which is only 0.178.

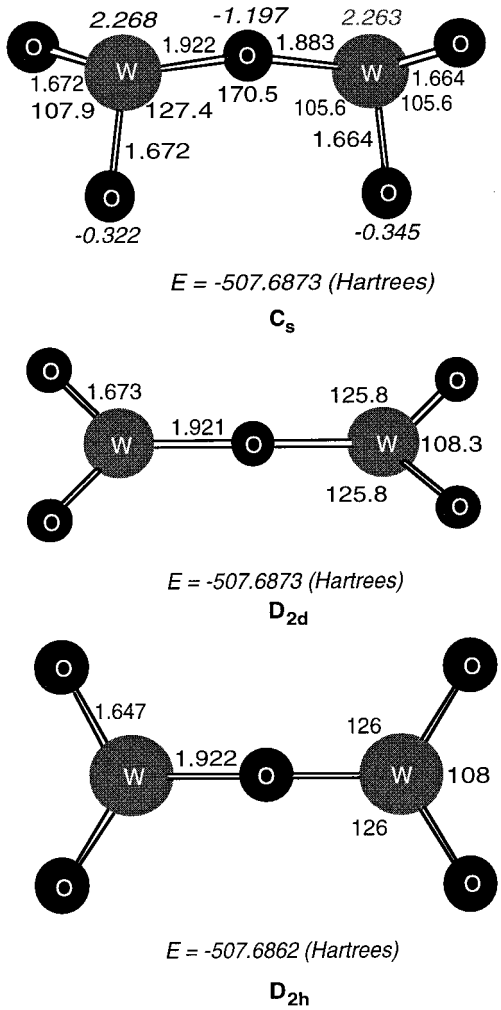

Figure 2. Structures of the C_s transition state and the D_{2d} and D_{2h} second- and third-order saddle points in the potential energy hypersurface of the $W_2O_5^{2+}$ dication (bond lengths in Å, bond angles in degrees).

TABLE 5: Geometrical, Energetic, and Electronic Properties of the Ground State $W_2O_6(D_{2h})$ Species Calculated at Various Levels of Theory

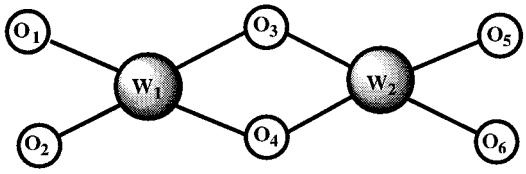

property	HF	MP2	B3LYP	QCISD(T)
$r(W_1-O_1)$ (Å)	1.693	1.798	1.730	
$r(W_1-O_3)$ (Å)	1.930	1.993	1.948	
$\angle W_1O_3W_2$ (°)	100.9	94.9	98.3	
$\angle O_1W_1O_3$ (°)	116.2	115.9	115.9	
$\angle O_3W_1O_4$ (°)	79.1	85.1	81.7	
$\angle O_1W_1O_3W_2$ (°)	113.9	116.5	114.8	
energy (Hartree)	−583.4835	−584.9099	−587.2543	−584.7701
ZPE (kcal/mol)	13.36	10.95	12.11	
q(W)	2.127	2.074	1.479	2.074
$q(O_1)$	−0.573	−0.578	−0.401	−0.578
$q(O_2)$	−0.982	−0.918	−0.677	−0.918

The bond overlap between the tungsten atoms is −0.539, showing a strong antibonding character and indicating that no metal−metal interactions are present in the $W_2O_6(D_{2h})$ molecule.

The formation of W_2O_6 from dimerization of the WO_3 moiety according to the following path

$$WO_3 + WO_3 \rightarrow W_2O_6$$

is predicted to be exothermic, the energy of formation being equal to 127.8, 100.3, 107.6, and 109.1 kcal·mol^{-1} at the HF, MP2, B3LYP, and QCISD(T) levels, respectively.

The most intense B_{3u} normal vibrational mode at 685.8 cm^{-1} (B3LYP results) corresponds to a skeletal deformation, while the intense B_{3u} normal mode at 1008.2 cm^{-1} could be tentatively assigned to a wagging vibration. The B_{3u} normal vibrational mode at 982.5 cm^{-1} could be assigned to scissors vibration.

3.2. Electronic Transitions and Bonding Properties of Molecular Tungsten Oxide Clusters. In the framework of a localized representation of the bonding in molecular tungsten oxide clusters we can ascribe the interaction between tungsten and oxygen as between W^{6+} and O^{2-} ions with a considerable back donation of electrons from occupied sp AOs of the oxygen donor ligand to vacant d AOs of the W central atom.

The molecular tungsten oxide clusters in their ground states exhibit analogous frontier molecular orbital (FMO) patterns. The HOMOs correspond to ligand group orbitals exhibiting significant $O^{2-}(2p)$ character, while the LUMOs are mainly localized on the W central atom. Both HOMO and LUMO of the ground state $WO_4^{2-}(T_d)$ dianion are triply degenerate orbitals of t_2 symmetry. The HOMO−LUMO gap of the $WO_4Na_2(C_1)$ molecule is very close to that of the ground state $WO_4^{2-}(T_d)$ dianion, 0.18 eV vs 0.16 eV illustrating the highly ionic character of the interaction of the Na^+ ions with the oxygen atoms. Obviously, the clambing of the $WO_4^{2-}(T_d)$ dianion on the Na^+ ions has no effect on the nature and relative energy of the frontier molecular orbitals. Above LUMOs follow the ligand field bands of the molecular tungsten oxide clusters involving the antibonding ligand field orbitals with predominantly d orbital character, showing the expected splitting pattern for the particular symmetry of the respective ligand field. All of these orbitals along with the W 6s orbital are vacant orbitals for W^{6+}. Therefore, the only absorption band expected in the electronic spectra of the tungsten oxide clusters under consideration is an $O^{2-}(2p) \rightarrow W^{6+}(5d)$ UV absorption assigned to an interstate HOMO → LUMO LMCT excitation. The UV absorption band is predicted, by means of CI−singles (CIS) calculations, to be a composite band involving a number of electronic transitions with excitation energies and oscillator strengths given in Table 6. Our theoretical results strongly support the experimentally determined optical reflectance spectra of $n[WO_{3-x}]-Na_{56}Y$.[15,16] A ligand field band assigned to $W^{5+} \rightarrow W^{5+}$ ligand field excitation is predicted to occur around 405, 350, 520, and 650 nm for $WO_3(C_{3v})$, $WO_4^{2-}(T_d)$, $W_2O_5^{2+}(C_1)$, and $W_2O_6(D_{2h})$, respectively. Obviously, the ligand field band assigned to $W^{5+} \rightarrow W^{5+}$ ligand field excitation of $WO_4^{2-}(T_d)$ dianion around 350 nm shifts into the UV region, where it could overlap with the intense UV-LMCT band. The computed ligand field parameter Δ_{Td} for the $WO_4^{2-}(T_d)$ dianion amounts to about 29 700 cm^{-1} at the B3LYP level of theory. It should be noted that the molecular orbital energy level diagrams of the ground state $WO_4^{2-}(T_d)$, $W_2O_5^{2+}(C_1)$, and $W_2O_6(D_{2h})$ molecules resemble the qualitative miniband electronic scheme for 16-$[WO_3]-Na_{56}Y$ species suggested by Ozin et al.[15,16] Finally, both protonation and clambing of the $WO_4^{2-}(T_d)$ dianion to Na^+ ions shift the UV absorption bands toward higher wavelengths.

3.3. GIAO Magnetic Shielding Tensor Elements of Molecular Tungsten Oxide Clusters. Employing gradient-corrected levels of DFT ^{183}W, ^{17}O, ^{23}Na, and ^{1}H chemical shifts were calculated at the GIAO-B3LYP level of theory. The computed ^{183}W, ^{17}O, ^{23}Na, and ^{1}H isotropic shielding tensor

TABLE 6: Computed Excitation Energies (nm) and Oscillator Strengths (in parentheses) of the Molecular Tungsten Oxide Clusters

$WO_3(C_{3v})$	$WO_4^{2-}(T_d)$	$WO_4H_2(C_2)$	$WO_4Na_2(C_1)$	$W_2O_5^{2+}(C_1)$	$W_2O_6(D_{2h})$
328.33 (0.000)	189.47 (0.000)	227.86 (0.001)	213.58 (0.000)	318.58 (0.001)	259.57 (0.016)
316.44 (0.018)	177.76 (0.000)	205.63 (0.000)	207.08 (0.004)	318.09 (0.001)	257.82 (0.000)
280.37 (0.000)	177.26 (0.000)	200.92 (0.000)	195.53 (0.000)	303.87 (0.003)	253.54 (0.041)
271.82 (0.011)	177.00 (0.000)	190.17 (0.000)	193.06 (0.016)	303.28 (0.000)	248.11 (0.000)
236.26 (0.021)		188.38 (0.013)	186.04 (0.008)	262.15 (0.015)	247.19 (0.000)
233.14 (0.036)		185.06 (0.000)	183.60 (0.007)	259.76 (0.006)	246.87 (0.000)
		182.73 (0.005)	182.81 (0.003)	258.74 (0.016)	242.20 (0.000)
		177.84 (0.000)	181.89 (0.003)		221.71 (0.000)

TABLE 7: ^{183}W, ^{17}O, ^{23}Na, and ^{1}H Magnetic Isotropic Shielding Tensor Elements (δ, ppm) along with Corresponding Anisotropies (in parentheses) of the Molecular Tungsten Oxide Clusters Computed at the GIAO-B3LYP Level

		^{17}O					
	^{183}W	(terminal)	(bridged)	(triply bridged)	^{17}OH	^{1}H	^{23}Na
$WO_3(C_{3v})$	−228 (80)	−702 (674)					
$WO_4^{2-}(T_d)$	−160 (0)	−206 (202)					
$WO_4H_2(C_2)$	−142 (69)	−548 (647)			129 (124)	27 (7)	
$WO_4Na_2(C_1)$	−126 (12)	−438 (399)	−238 (224)	−24 (76)			0.7 (1.4)
$W_2O_5^{2+}(C_1)$	−251 (68)	−1089 (1137)	−200 (104)				
		(−1059) (1144)					
$W_2O_6(D_{2h})$	−199 (60)	−751 (714)	−291 (172)				

elements (δ, ppm) along with corresponding anisotropies for the ground state molecular tungsten oxide clusters are summarized in Table 7. ^{183}W chemical shifts (δ, ppm) for the Keggin polyoxo anion $[(H_2)_2\{W_3^{IV}(OH_2)_3\}W_9^{VI}O_{34}(OH)_3]^{3-}$ have recently been determined experimentally.[26] It is clear that the computed value of the ^{183}W chemical shift of $WO_3(C_{3v})$ is very close to those corresponding to W^{6+} ions with an analogous environment in the polyoxo anion (e.g., −171.0 and −187.4 ppm for W_F and W_G, respectively). For the trigonal planar (D_{3h}) transition state the computed ^{183}W and ^{17}O isotropic shielding tensor elements are −361 and −1173 respectively with corresponding anisotropies of 279 and 1082 ppm. It is evident that the NMR chemical shifts are strongly influenced by the stereochemistry of the molecule. In effect the paramagnetic component of the magnetic shielding tensor σ^p is more sensitive to structural changes than the diamagnetic σ^d one. The diamagnetic shielding σ^d is positive and dominated by the contributions from core density, while σ^p is negative and dominated by the occupied-virtual contributions. It is evident then why σ^p is more sensitive to structural changes than is σ^d.

The computed ^{183}W and ^{17}O isotropic shielding tensor elements (δ, ppm) for the ground state WO_4^{2-} (T_d) dianion at the GIAO-B3LYP level of theory are in excellent agreement with those computed recently by Schreckenbach and Ziegler[27,28] for the $WO_4^{2-}(T_d)$ dianion at a DFT-GIAO level of theory. For the square planar (D_{4h}) transition state, the computed ^{183}W and ^{17}O isotropic shielding tensor elements are −190 and 2019, respectively, with corresponding anisotropies of 455 and 7409 ppm. For the $WO_4^{2-}(T_d)$ species it is also evident that the coordination geometry strongly affects the isotropic magnetic shielding tensor of the coordinated O donor atoms. The protonation of the $WO_4^{2-}(T_d)$ dianion results in a significant shielding of ^{17}O and particularly the protonated ones (^{17}OH).

The computed ^{183}W isotropic magnetic shielding tensor of $WO_4Na_2(C_1)$ is in line with the experimentally determined[26] value of −128.7 ppm for W_E of the Keggin polyoxo anion $[(H_2)_2\{W_3^{IV}(OH_2)_3\}W_9^{VI}O_{34}(OH)_3]^{3-}$. There is a downfield shift of the ^{17}O chemical shifts upon increasing the number of atoms surrounding the oxygen atoms, e.g., going from the terminal to bridged and triply bridged oxygen atoms, in line with the increased negative net atomic charges on the respective oxygen atoms. Most important is the excellent agreement of the computed ^{23}Na chemical shifts (δ, ppm) of $WO_4Na_2(C_1)$ to those determined experimentally[16,17] for various tungsten oxides encapsulated in sodium zeolite Y. The high-resolution ^{23}Na DOR resonances depending on the loading of the zeolite with the tungsten oxides occur at around −18 ppm for the samples loaded with 16 or more WO_2 monomers/unit cell and at around 0 ppm for the samples loaded with 8 WO_2 monomers/unit cell. In the latter case the encapsulated WO_4^{2-} tetrahedra are closer to our model of the isolated WO_4^{2-} tetrahedral unit.

The bridging oxygen atom in the $W_2O_5^{2+}(C_1)$ dication is more shielded with respect to the terminal ones, with the latter being magnetically nonequivalent. The ^{183}W atoms in the $W_2O_5^{2+}$-(C_1) dication are deshielded with respect to those of the WO_3 and WO_4^{2-} species. The bridging μ-^{17}O atom of the $W_2O_6(D_{2h})$-moiety is also more shielded than the terminal ^{17}O atoms. The ^{183}W and the terminal ^{17}O atoms in the $W_2O_6(D_{2h})$ moiety are shielded with respect to those of the $W_2O_5^{2+}$ species. In contrast, the μ-^{17}O atoms are deshielded with respect to those of the $W_2O_5^{2+}$ species.

Conclusions

The use of first principles computational techniques in the study of small tungsten oxide clusters yielded some interesting results. Beginning with the WO_3 species it is predicted to possess a trigonal pyramidal structure of C_{3v} symmetry. The trigonal planar structure of D_{3h} symmetry corresponds to the transition state for the inversion process of the C_{3v} molecule. The WO_4^{2-} dianion adopts a T_d configuration. The square planar structure of D_{4h} symmetry corresponds to the transition state for a possible reaction pathway of the inversion process of the T_d molecule. Upon protonation the dianion affords the neutral dihydroxy molecule exhibiting a C_2 configuration. The protonation results in the lengthening of the protonated W−O bonds, as well as a significant charge redistribution reflected in the increase of the net positive charge on the metal followed by a concomitant decrease of the net negative atomic charge on the terminal oxygen atoms. The clambing of the $WO_4^{2-}(T_d)$ dianion through oxygen atoms to Na^+ ions lowers the symmetry of the $WO_4^{2-}(T_d)$ dianion to C_1. Interestingly, the WO_4^{2-} dianion bonds to two Na^+ ions in an η^2-type of bonding sharing a common oxygen atom with the O−Na bond being predominantly ionic. The triply bridged oxygen atom acquires the higher negative

net atomic charge. The $W_2O_5^{2+}$ dication adopts a C_1 configuration. The topomer belonging to C_s symmetry possesses one imaginary frequency and is a rotational transition state to the C_1 topomer. The most stable configuration of the W_2O_6 is that belonging to the D_{2h} point group. The formation of the W_2O_6 from the dimerization of WO_3 is predicted to be exothermic. The structural, energetic, electronic, and magnetic properties of all tungsten oxides studied have been computed and compared to experimental and theoretical data where available. However, in most cases the results are predictions.

Acknowledgment. We are grateful to the General Secretariat of Research and Technology of the Greek Ministry of Industry, Energy and Technology for support of this work (Grant No. 980, ΠΕΝΕΔ95).

References and Notes

(1) Merer, A. J. *Annu. Rev. Phys. Chem.* **1989**, *40*, 407.
(2) Kaldor, A.; Cox, D. M.; Zakin, M. R. *Adv. Chem. Phys.* **1988**, *70*, 221.
(3) Jena, P., Rao, B. K., Khanna, S. N., Eds. *Physics and Chemistry of Small Clusters*; Plenum: New York, 1987.
(4) Tranger, F., Putlitz, G. Z., Eds. *Metal Clusters*; Springer-Verlag: Berlin, 1986.
(5) Russell, D. H., Ed. *Gas-Phase Inorganic Chemistry*; Plenum: New York, 1989.
(6) Castleman, A. W., Jr.; Keesee R. G. *Chem. Rev. Phys. Chem.* **1986**, *86*, 589.
(7) Ai, M. *J. Catal.* **1977**, *49*, 305.
(8) Yamaguchi, L.; Tanaka, Y.; Tanabe, K. *J. Catal.* **1980**, *65*, 442.
(9) Lietti, T.; Tanaka, Y.; Svachula, J.; Forzatti, P.; Busca, G.; Ramis, G.; Bregani, F. *Catal. Today* **1993**, *17*, 131.
(10) Salje, E. *J. Appl. Crystallogr.* **1974**, *7*, 615.
(11) Cora, F.; Patel, A.; Harrison, N. M.; Dovesi, R.; Catlow, C. R. A. *J. Am. Chem. Soc.* **1996**, *118*, 12174.
(12) Sienko, M. J. In *Non-Stoichiometric Compounds*; Gould, R. F., Ed.; Advances in Chemistry Series; American Chemical Society: Washington, D.C., 1963.
(13) Dickens, P. G.; Whittingham, M. S. Q. *Rev. Chem. Soc* **1968**, *22*, 30.
(14) Cora, F.; Lewis, D. W.; Catlow, C. R. A. *J. Chem. Soc., Chem. Commun.* **1998**, 1943.
(15) Ozin, G. A.; Özkar, S.; Prokopowicz, R. A. *Acc. Chem. Res.* **1992**, *25*, 553.
(16) Ozin, G. A.; Prokopowicz, R. A.; Özkar, S. *J. Am. Chem. Soc.* **1992**, *114*, 8953.
(17) Jelinek, R.; Özkar, S.; Ozin, G. A. *J. Phys. Chem.* **1992**, *92*, 5949.
(18) Pastore, H. O.; Ozin, G. A.; Poé A. J. *J. Am. Chem. Soc.* **1993**, *115*, 1215.
(19) Frisch, M. J.; Trucks, G. W.; Schlegel, H. B.; Gill, P. M. W.; Johnson, B. G.; Robb, M. A.; Cheeseman, J. R.; Keith, T.; Petersson, G. A.; Montgomery, J. A.; Raghavachari, K.; Al-Laham, M. A.; Zakrzewski, V. G.; Ortiz, J. V.; Foresman, J. B.; Cioslowski, J.; Stefanov, B. B.; Nanayakkara, A.; Challacombe, M.; Peng, C. Y.; Ayala, P. Y.; Chen, W.; Wong, M. W.; Andres, J. L.; Replogle, E. S.; Gomperts, R.; Martin, R. L.; Fox, D. J.; Binkley, J. S.; Defrees, D. J.; Baker, J.; Stewart, J. P.; Head-Gordon, M.; Gonzalez, C.; Pople, J. A. *Gaussian 94*, revision D4; Gaussian, Inc.: Pittsburgh, PA, 1995.
(20) Loopsta, B. O.; Rietveld, H. M. *Acta Crystallogr.* **1969**, *B25*, 1420.
(21) Tanisaki, S. *J. Phys. Chem. Soc. Jpn.* **1960**, *15*, 573.
(22) Loopsta, B. O.; Boldrini, P. *Acta Crystallogr.* **1966**, *21*, 158.
(23) Stashans, A.; Lunell, S. *Int. J. Quantum Chem.* **1997**, *63*, 729.
(24) Corà, F.; Patel, A.; Harrison, N. M.; Dovesi, R.; Catlow C. R. A. *J. Am. Chem. Soc.* **1996**, *118*, 12174.
(25) Veliah, S.; Xiang, K.; Pandey, R.; Recio, J. M.; Newsam, J. M. *J. Phys. Chem. B* **1998**, *102*, 1126.
(26) Boskovic, C.; Sadek, M.; Brownlee, R. T. C.; Bond, A. M.; Wedd A. G. *J. Chem. Soc., Chem. Commun.* **1999**, 533.
(27) Schreckenbach, G.; Ziegler, T. *Int. J. Quantum Chem.* **1997**, *61*, 899.
(28) Schreckenbach, G.; Ziegler, T. *Theor. Chem. Acc.* **1998**, *99*, 71.